RSC Advances

PAPER

View Article Online
View Journal | View Issue

Cite this: *RSC Adv.*, 2015, **5**, 66650

Hybrid bismuth oxyhalides@gypsum as self-cleaning composites: novel aspects of a sustainable photocatalytic technology for solar environmental cleanup†

Hani Gnayem,*[a] Vladimir Uvarov,[b] Ofer Lahad[a] and Yoel Sasson*[a]

Received 27th May 2015
Accepted 29th July 2015

DOI: 10.1039/c5ra09993e

www.rsc.org/advances

Herein we report the fabrication of a novel heterojunctioned $BiOCl_xBr_{1-x}$@gypsum composite and its application as a self-cleaning surface for the straightforward use in construction and building materials. The morphology, chemical composition and crystal structure of the hybrid material were characterized using X-ray diffraction and scanning electron microscopy. The photocatalytic activity of the new composite was investigated for the degradation of naphthalene and rhodamine B (RhB) under visible light ($\lambda \geq 420$ nm) irradiation. Our results show rapid and complete destruction of the RhB dye after only 4 minutes under Xe visible light irradiation (422–740 nm) and 2.5 minutes under mild sunlight illumination. Total organic carbon measurements could verify the absolute mineralization of the recalcitrant naphthalene contamination, as a state of the art example, within 20 minutes of visible light illumination.

1. Introduction

Scientists are nowadays facing major challenges in countering air, water and soil pollution. Of particular interest is conceiving ways to decompose organic materials and mould deposited on building surfaces, which are responsible for the deterioration of their appearance. Inorganic semi-conductor based photocatalysts applied as coatings on buildings and stone structures can be a motivating solution in order to lower maintenance costs by reducing surface soiling and the need for costly cleaning operations.[1]

In the field of photocatalytic construction and building materials, titanium dioxide (TiO_2) is the most widely used substance which has been used as a white pigment in paints, cosmetics and foodstuff since ancient times.[2]

The use of photocatalysts blended with building materials started from the early 1990s. The versatile function of TiO_2, which can serve as a photocatalyst and as a structural material, has facilitated its application as an exterior construction component and an interior furnishing matter, combined with *e.g.* cement mortar, exterior tiles, paving blocks, glass and PVC fabric.

Despite the intensity and diffusion of these studies,[3–7] there were no major practical breakthroughs in the field.

The oxidative properties of titanium dioxide were utilized to achieve self-cleaning surfaces by means of solar light[8] and, in parallel, it was sought to use the capacity of the aforementioned oxide combined with ultraviolet radiation, to transform surfaces into highly hydrophilic textures, so rain contributes to their cleaning.[9] These applications had a reasonable commercial success. In what seems to be the beginning of a new era of photocatalysis, recent work oriented toward the use of *visible light* to drive chemical processes. The approach is to modify the catalyst properties by varying the chemical composition so it can be activated by the visible broader spectrum of the sun. In addition to diverse applications in the fields of air, water and wastewater treatment, heterogeneous photocatalytic oxidation is central for self-cleaning purposes.[10,11]

Consequently a smart and elegant application of solid-state semiconductors photocatalysis is its application in construction and building materials. Given their large surface areas, buildings can conveniently be used to promote the elimination of organic pollutant gases from the surrounding air.

To protect the surfaces of cementitious materials and minimize the negative influence of environment conditions on buildings, the advanced oxidation processes such as heterogeneous photocatalysis started to play a major role in building industry.[12–14]

Recently, bismuth oxyhalides have received considerable attention and are of immense significance due to their excellent visible light photocatalytic activity.[15–19]

[a]*Casali Center of Applied Chemistry, The Institute of Chemistry, The Hebrew University of Jerusalem, Jerusalem 91904, Israel. E-mail: ysasson@huji.ac.il; hani.gnayem@mail.huji.ac.il; Fax: +972 2652 9626; Tel: +972 6584530/+972 2658 6567*

[b]*The Unit for Nanoscopic Characterization, The Center for Nanoscience and Nanotechnology, The Hebrew University of Jerusalem, Jerusalem 91904, Israel*

† Electronic supplementary information (ESI) available: Table S1: solid TOC measurements, Fig. S1: BET surface area isotherm of the investigated alloy. See DOI: 10.1039/c5ra09993e

As a ternary oxide semiconductor, BiOX (X = F, Cl, Br, I) comprises a layered crystal structure consisted of tetragonal $[Bi_2O_2]^{2+}$ positive slabs interleaved by double negative slabs of halogen atoms along the *c* axis. Their outstanding optical, light harvesting and electrical properties render them promising substances for applications as pharmaceuticals,[20] pigments[21] and catalysts[22] as well as gas sensing materials.[23]

Herewith, as a first novel study discussing BiOX family of materials *for self-cleaning purposes*, we report the facile and straightforward integration of $BiOCl_xBr_{1-x}$ ($0 \leq x \leq 1$) solid solutions[19] in construction materials while focusing on gypsum ($Ca(SO_4)\cdot 2H_2O$) as an archetypal candidate.

Rhodamine B (RhB) and naphthalene were selected for probing and evaluating the photodestruction capacity of the above alloys while being incorporated into gypsum surfaces.

The fabricated $BiOCl_xBr_{1-x}$@gypsum formulations were exposed to visible light irradiation using Xe arc lamp, natural afternoon sunlight as well as simple battery-powered LED lamps.

2. Experimental section

2.1 Materials and methods: catalysts and gypsum integrated composites-preparation and characterization

Materials. All materials were purchased from Aldrich-Sigma and were used without further purification.

Preparation of $BiOCl_{0.8}Br_{0.2}$ solid-solution. Deionized water (75 mL), glacial acetic acid (35 mL) and bismuth nitrate (9.18 g) are added to a flask and mixed at room temperature for fifteen minutes until a clear, transparent solution is formed. Cetyltrimethylammonium bromide-CTAB (1.378 g dissolved in 10 mL of water) and cetyltrimethylammonium chloride-CTAC (4.85 g in the form of 25 wt% aqueous solution) are added to the solution, for additional 30 minutes of mixing at room temperature. The white precipitate thus formed is separated from the liquid phase by filtration, washed five times with ethanol (20 mL) and five times with water (50 mL), in order to remove the non-reactive organic species. The solid is then dried (in air). The weight of the solid collected is 7 g (yield = 91%).

Gypsum composites. The $BiOCl_xBr_{1-x}$@gypsum composites used in this study were prepared by mixing the commercially available Tambour gypsum with stoichiometric amount of distilled water followed by spaying the $BiOCl_{0.8}Br_{0.2}$ photocatalyst. Composites with 1, 2 and 4 wt% of the photocatalyst were prepared and applied as material for coating of gypsum plates using commercial spray coater. These plates were used for both structural and photocatalytic studies.

Sustainable aspects of the synthetic protocol: recycle of raw materials. The *filtrate formed* in the above procedure contains some major ingredients of the process and can be easily recycled. These are water, acetic acid and particularly the quaternary ammonium salts (probably with nitrate counter anion). This filtrate can directly serve as a reaction medium for the successive batch. It is easily regenerated; fresh amounts of the reactants which were consumed in the reaction are added to the filtrate, except for the quaternary ammonium salt surfactant whose activity as structure-directing agent can be restored in a satisfactory manner by means of an addition of a water soluble halide salt. Thus, the bismuth salt is fed to the filtrate together with water-soluble halide salt (*e.g.*, alkali halide such as sodium chloride and potassium bromide) and the regenerated filtrate is supplied to the next production batch for use as a reaction medium. The products which are formed in a fresh or a recycled reaction medium are equally excellent in respect of their photocatalytic activity. The process of the invention is hence readily applicable for large scale production either in a batch or continuous mode of operation.

2.2 Characterization

X-ray powder diffraction measurements were performed on the D8 Advance diffractometer (Bruker AXS, Karlsruhe, Germany) with a goniometer radius 217.5 mm, secondary graphite monochromator, 2° Sollers slits and 0.2 mm receiving slit. XRD patterns within the range 5° to 70° 2θ were recorded at room temperature using CuKα radiation ($\lambda = 1.5418$ Å) with following measurement conditions: tube voltage of 40 kV, tube current of 40 mA, step-scan mode with a step size of 0.02° 2θ and counting time of 1 s per step. Gypsum plasters coated by $BiOCl_{0.8}Br_{0.2}$ were located on sample stage that is regulated along the vertical axis, and allows obtaining XRD patterns from as-manufactured samples with various sizes. Uncoated material of plaster was grinded in agate mortar to powder and placed into low-background quartz sample holders.

Morphological observations and chemical analysis were performed using Environmental Scanning Electron Microscope (ESEM) Quanta 200 (FEI, Eindhoven, Netherlands) equipped with EDS detector (EDAX-TSL, USA) and operated in low vacuum mode (0.6 Torr pressure) at 20 kV accelerating voltage, and with the High Resolution Scanning Electron Microscope (HR SEM) Sirion (FEI, Eindhoven, Netherlands) in Ultra-High resolution mode with Through the Lens Detector. Accelerating voltage and working distance were set at 5 kV and 5 mm correspondingly.

Diffuse Reflectance Analysis was carried out by Integrating Sphere (JASCO V-650 Series ISV-722).

Surface area was determined by the N2 Brunauer–Emmett–Teller (BET) method (NOVA-1200e).

Total Organic Carbon (TOC) measurements have been conducted using SKALAR PRIMACS^{SLC} Solid TOC ANALYZER. Model no. 2CS22901.

3. Results and discussion

3.1 Material characterization

Fig. 1 shows the XRD patterns acquired from as-synthesized $BiO(Cl_xBr_{1-x})$ sample, from coated gypsum plaster and from pure gypsum (for comparison). Fig. 1b shows XRD pattern obtained from coated gypsum plaster, and diffraction peaks of both phases ($BiOCl_{0.8}Br_{0.2}$ and gypsum) are clearly visible. Analysis of the XRD pattern (Fig. 1b) revealed that one of the crystal phases is $BiOCl_xBr_{1-x}$ (unit cell parameters $a = b = 3.89$ Å, $c = 7.484$ Å, *P4/nmm* (no. 129) space group), and second phase is gypsum $Ca(SO_4)\cdot 2H_2O$. The composition of photocatalyst was calculated as described in our recent works[19,24] using value of

the c-parameter obtained from XRD data *via* $x = 10.966 - 1.354c$ (x is content of chlorine). We obtained $x = 0.81$ that is very close to the claimed composition of the photocatalyst. Moreover, very broad $BiOCl_{0.8}Br_{0.2}$ peaks indicate the nanosize of its crystallites. The crystallite sizes of $BiOCl_{0.8}Br_{0.2}$ photocatalyst calculated using Scherrer equation were about 8 nm.

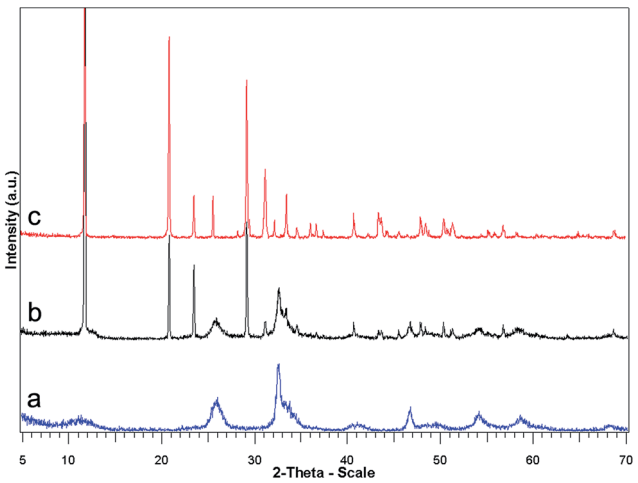

Fig. 1 XRD patterns acquired from as-synthesized $BiOCl_{0.8}Br_{0.2}$ nanoparticles (a), $BiOCl_{0.8}Br_{0.2}$ layer on gypsum (b) and pure gypsum (c).

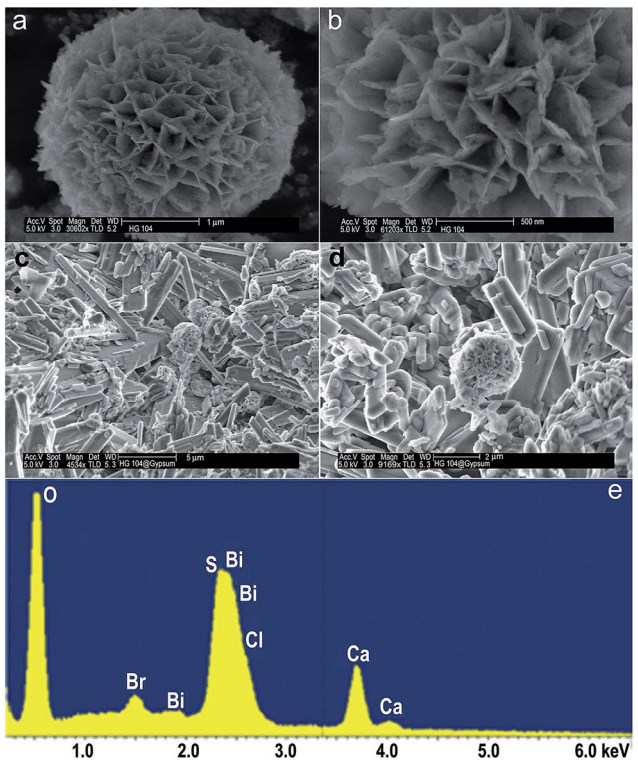

Fig. 2 SEM images acquired from dry powders of as-synthesized $BiOCl_{0.8}Br_{0.2}$ (a and b) and from coated gypsum surface (c and d). EDS spectrum (e) was acquired from coated surface at 30 kV accelerating voltage.

Fig. 2 shows images acquired from dry as-synthesized $BiOCl_{0.8}Br_{0.2}$ and from the same material on gypsum surface. Imaging in secondary electrons (Fig. 2a and b) revealed topographical details of the observed morphology. As is seen in Fig. 2, $BiOCl_{0.8}Br_{0.2}$ particles have a shape of microspheres with a size about 3 μm, which are built of thin plates having lateral dimensions of hundreds of nanometers. Although the lateral dimensions of plates were about hundreds of nanometers, their thickness was about 10 nm only. On gypsum surface we see both $BiOCl_{0.8}Br_{0.2}$ microspheres and their component plates (Fig. 2c and d). Elongated crystals of gypsum are also perfectly visible. The adduced EDS spectrum confirms the chemical composition of the material.

To verify the location of $BiOCl_{0.8}Br_{0.2}$ we analyzed cross sectional samples of the coated material with EDS in SEM. We found that $BiOCl_{0.8}Br_{0.2}$ is absent in the bulk of the plaster while it is present in the superficial layer. The SEM image obtained from cross-sectional sample is shown in Fig. 3. As is clearly seen from Fig. 3, $BiOCl_{0.8}Br_{0.2}$ photocatalyst is composed of micron size particles exhibiting very strong contrast at back scattered electron (BSE) imaging. The thickness of coating layer is about 50–80 μm. EDS spectra acquired from the marked areas are shown in the in Fig. 3. The EDS analysis confirms that the plaster material beneath the coating layer is gypsum. A weak calcium peak appears in the EDS spectra acquired at coated regions (brown line) and indicates presence of gypsum in the coated layer, but in the latter the gypsum content is much less than in the plaster body.

3.2 Photocatalytic activity

Once a pollutant has been deposited, its disappearance and those of its degradation intermediate products can be followed with various techniques. The cleaning efficacy is best evaluated by optical methods, particularly when stains are studied.

Successive pictures can also be taken and analyzed by graphical modeling. These optical measurements have obviously the interest of taking into account the effects on the visual aspect of both the initially deposited compound(s) and the degradation intermediate products. As was aforementioned, the variations in color can be quantified when the deposited compound is a dye.

For these reasons we have evaluated the photocatalytic degradation of RhB (30 ppm) dye sprayed on the prepared $BiOCl_xBr_{1-x}$@gypsum composites while exposing the later to various irradiation sources, at different day times, including natural sunlight and 300 W Xe arc lamp (Max-302, Asahi spectra). Power consumption of Max-302 is 500 VA.

For visible light experiments a 422 nm cut-off filter was used. The light intensity was fixed at 70 mW cm^{-2} and the samples were placed 10 cm away from the light's source mirror.

The fabricated well-dried coated gypsum plates were contaminated by an aqueous solution containing 30 ppm of RhB, simply by trickling 10 drops of the dye solution on the center of the tested surfaces. These contaminated $BiOCl_{0.8}Br_{0.2}$@gypsum composites were kept for 60 min on dark thus the adsorption–desorption equilibrium of RhB stain will be

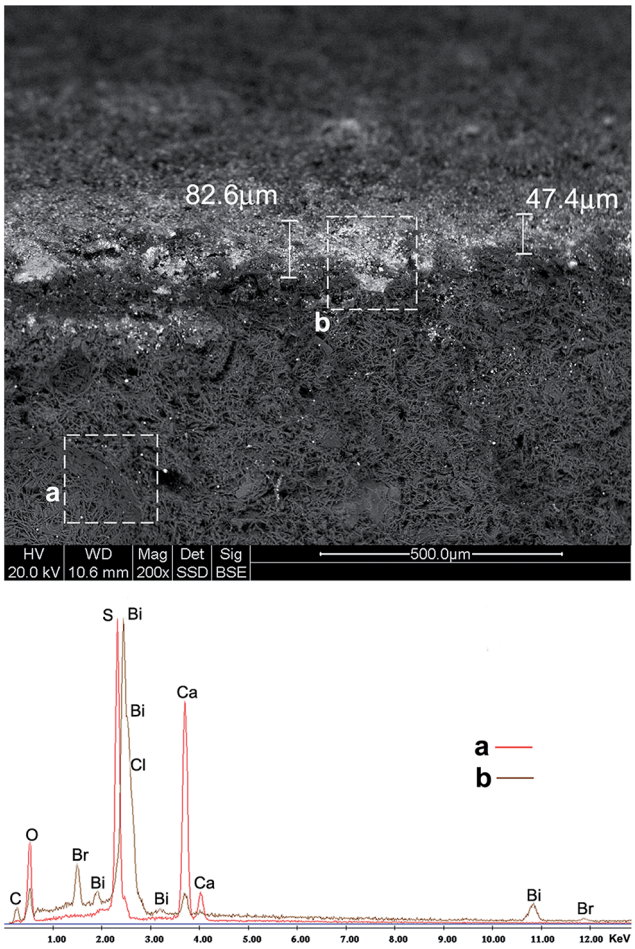

Fig. 3 SEM image and EDS spectra acquired from the cross-section sample. The areas from which the EDS spectra were acquired are marked with dashed squares. The EDS spectrum acquired from the top region (the upper dashed square) is shown as a brown line, while that of the plaster region (the lower dashed square) is shown as a red line.

completely accomplished. Subsequently, the photolysis and photocatalytic capacities were warily evaluated.

Fig. 4a & b refer respectively to the dark adsorption–desorption equilibrium and photolysis processes of uncoated gypsum plates. The later were used as blank and contrast experiments. Fig. 4b shows the photolysis of the RhB stain after 4 minutes of irradiation under Xe lamp (422–740 nm). As it can be effortlessly guaranteed, the photolysis of the dye is confidently negligible.

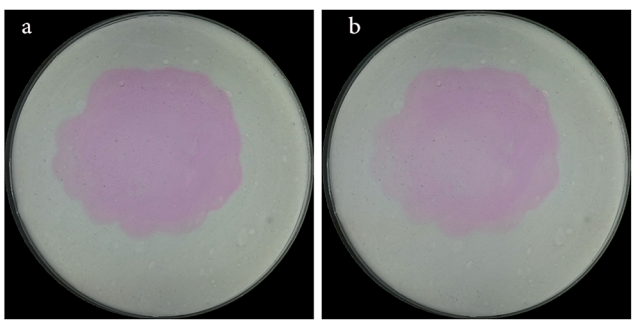

Fig. 4 (a) Dark adsorption–desorption equilibrium and (b) photolysis of RhB over uncoated gypsum plate under Xe visible light illumination.

Fig. 5 demonstrates the gradual photocatalytic decomposition of a RhB stain over $BiOCl_{0.8}Br_{0.2}$@gypsum (2 wt%) composite under Xe lamp visible light irradiation ($\lambda = 422$–740 nm). The clear-cut disappearance of the dye stain is undoubtedly observed and can be easily and visually monitored by naked eye. Nine images have been taken for recording the photodegradation processes with time interval of 0.5 min between one image to the next one. As it is clearly shown, the complete and swift destruction of the RhB dye could be successfully achieved within only 4 minutes of irradiation.

Fig. 6 elucidates the swift photo-oxidation of the RhB dye over $BiOCl_{0.8}Br_{0.2}$@gypsum (2 wt%) composite while exposing the surface to natural afternoon solar light. Complete self-cleaning is monitored after 2.5 minutes of illumination.

It is of utmost importance to clarify that there was no significant difference (in terms of kinetic rates) in the photocatalytic efficacy between the samples containing 2 and 4 wt% of photocatalyst, thus indicating that even a minor portion (>1 wt%) of well dispersed powerful photocatalyst is unequivocally sufficient for fabricating a photostable light harvesting oxidative material.

The ultimate visible light driven photodecomposition of RhB contamination presented above was tested in numerous number of cycles without any loss in activity. Additionally, the prepared surfaces maintained their superb photocatalytic efficiency even after seven months since were first fabricated. Lastly, further experiments, conducted under the same conditions, using simple 11 W table lamp and even 6 W LED lamps demonstrated rapid photodestruction of RhB which was accomplished within less than 60 minutes of illumination.

Photodecomposition of naphthalene over $BiOCl_{0.8}Br_{0.2}$@ gypsum composite. Following the molecular photodecomposition of RhB shown above we have continued towards investigating the challenging photo-driven destruction of naphthalene.

Shedding a light on the mineralization of this specific colorless and persistent organic compound (photolysis under visible light is confidently negligible) underscores the practical highlights of semi-conductors based photocatalysis.

For this goal we have fabricated very thin surfaces (~1 mm) of gypsum coated with $BiOCl_{0.8}Br_{0.2}$ (2% W).

Simple mixing and molding of gypsum with stoichiometric amount of water inside Petri dish followed by spraying the photocatalyst has enabled a controlled deposition of our alloy on the curing gypsum.

In fact, these plates were created in a thin form in order to insure trustworthy solid TOC measurements as the complete content of the aforementioned surfaces has been utilized for carrying out the photodegradation analysis.

Two duplicates of hybrid $BiOCl_{0.8}Br_{0.2}$@gypsum were analyzed. The first one has been contaminated with naphthalene (~50 mg dissolved in EtOH, which has been later evaporated) and kept in the dark while the second identical sample

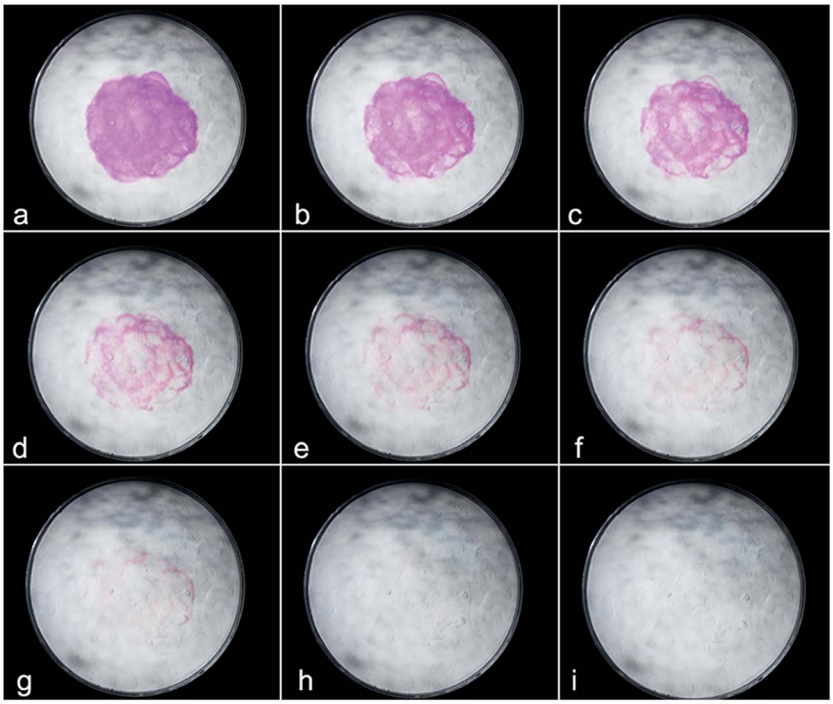

Fig. 5 Photodecomposition of RhB over $BiOCl_{0.8}Br_{0.2}$@gypsum under Xe visible light at 0.5 min time intervals while $a = 0$ min, $b = 0.5$ min, $c = 1$ min, $d = 1.5$ min, $e = 2$ min, $f = 2.5$ min, $g = 3$ min, $h = 3.5$ min, $i = 4$ minutes.

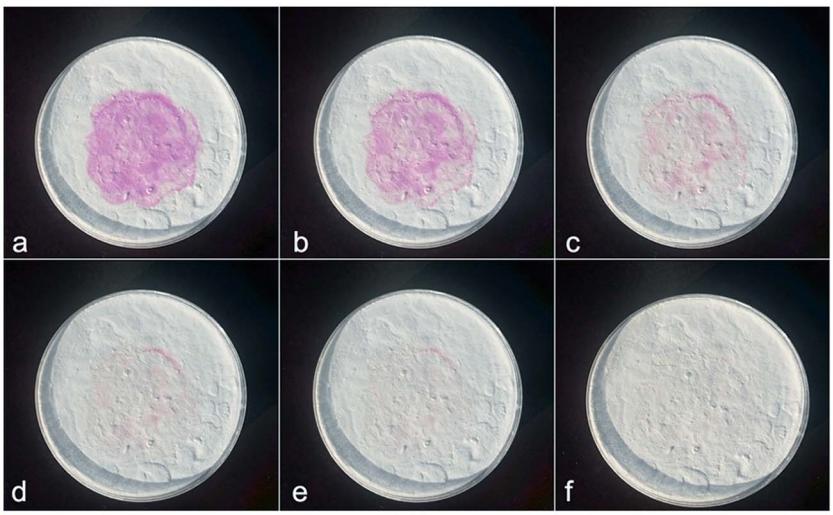

Fig. 6 Photodecomposition of RhB over $BiOCl_{0.8}Br_{0.2}$@gypsum under natural sunlight at 0.5 min time intervals while $a = 0$ min, $b = 0.5$ min, $c = 1$ min, $d = 1.5$ min, $e = 2$ min, $f = 2.5$ min.

has been illuminated with visible light (Xe, 422–740 nm) for 20 minutes prior to conducting the solid TOC analysis.

Fig. 7 depicts the solid total organic carbon measurements. The left peak shows the total content of organic carbon in the reference sample, namely before treatment. The right peak, designated as after treatment, indicates the same for the irradiated sample.

As it can be seen, over 90% decline in the TOC values was observed (for more details please see Table S1 in the ESI†).

3.3 Photophysical properties

Additional physical variables which are of supreme importance limiting the photoefficiency of semiconductors are the band gap and the conduction and valence band energy edges.

The determination of CB and VB edge electrochemical potentials of a semiconductor is essential in order to understand the photodegradation mechanism of pollutants. The bands edge positions of the photocatalyst were theoretically predicted using atom's Mulliken electronegativity definition:

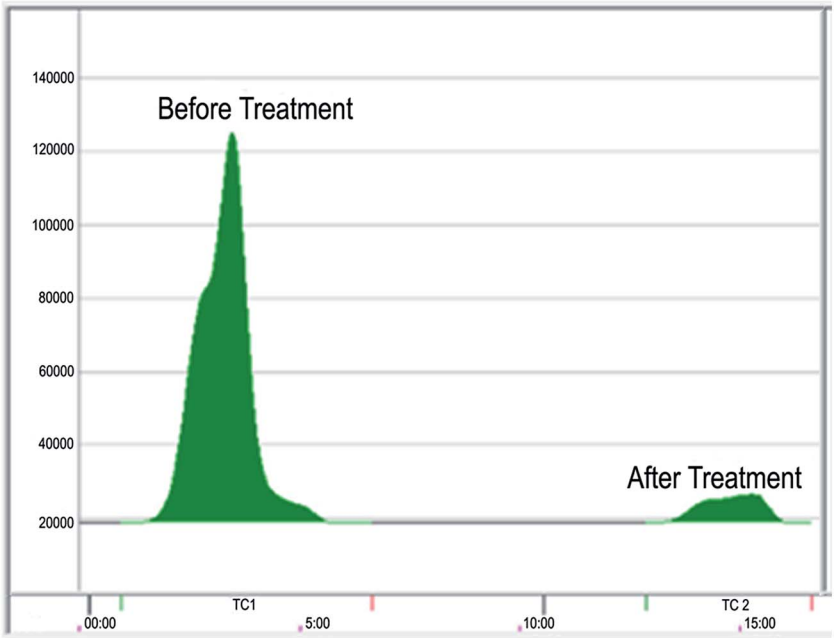

Fig. 7 TOC measurements of naphthalene over $BiOCl_{0.8}Br_{0.2}$@gypsum surfaces. Left peak illustrates the solid TOC measurement before treatment while the right peak belongs to the same after the controlled photodecomposition.

$$E_{VB} = \chi - E_e + 0.5E_g$$

where χ is the electronegativity of the semiconductor, E_e is the energy of free electrons on the hydrogen scale ($\approx$4.5 eV), and E_g is the band gap energy of the semiconductor.

According to this empirical expression, the calculated CB (E_{CB}), VB (E_{VB}) edge positions and the band gap of the sample estimated from the onsets of the absorption edge as shown in Fig. 8 (the diffuse reflectance spectrum of $BiOCl_{0.8}Br_{0.2}$) are:

$$(E_{CB}) = 0.36 \text{ eV}, (E_{VB}) = 2.96 \text{ eV}, (E_g) = 2.60 \text{ eV}.$$

Fig. 9 illustrates the band alignment, position of CB and VB of the studied semi-conductor.

The resultant BET isotherm of the as synthesised $BiOCl_{0.8}Br_{0.2}$ alloy is presented at the ESI (Fig. S1†). The recorded surface area according to this method is 25.75 $m^2\ g^{-1}$.

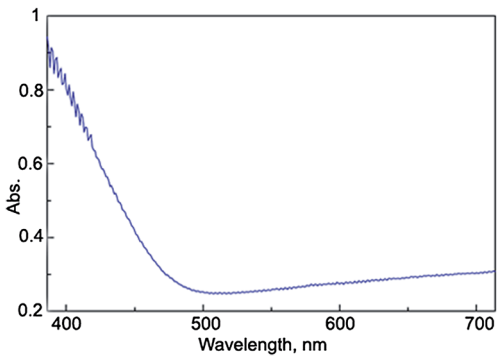

Fig. 8 The diffuse reflectance spectrum of $BiOCl_{0.8}Br_{0.2}$.

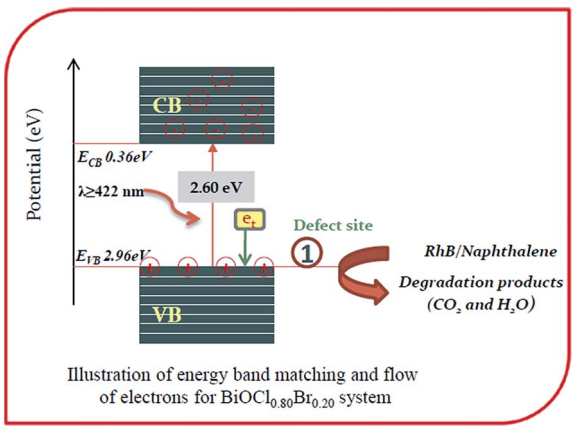

Fig. 9 A model of energy band matching and flow of electrons for $BiOCl_{0.80}Br_{0.20}$ system.

3.4 Mechanistic study

In order to detect the presence of OH˙ radical in $BiOCl_xBr_{1-x}$ photocatalyst we used terephthalic acid (TA) as a fluorescent probe. OH˙ radical is known to be trapped by TA to produce the fluorescent 2-hydroxyterephthalic acid.[25] There were no observable peaks when the $BiOCl_{0.8}Br_{0.2}$ suspensions were illuminated.

In another experiment, it was found that the addition of 2-propanol, as a scavenger of OH˙ radicals,[26] into the photoreaction system did not cause any noteworthy changes in the degradation rates of RhB and naphthalene.

Running the above experiment in the presence of benzoquinone, as a scavenger for super oxide anion, also had no

apparent effect on the reaction rate of the photodecomposition process.

In a valence band of Bi^{3+}, holes formed by photoexcitation[27] are regarded as Bi^{5+}. The standard redox potential of Bi^{V}/Bi^{III} is more negative than of $OH^{\bullet}/OH^{-}$.[28] Therefore, photogenerated holes on the surface of $BiOCl_xBr_{1-x}$ are not expected to react with OH^{-}/H_2O to form $OH^{\bullet}$, suggesting that the decomposition of RhB could be attributed mainly to a direct photo-oxidation reaction with the photogenerated holes.[29]

4. Conclusions

In the present study, we demonstrate a potent self-cleaning featured composite based on photocatalytic $BiOCl_{0.8}Br_{0.2}$ semi-conductor and commercially available gypsum. Since this form of $Ca(SO_4)\cdot 2H_2O$ is utilized in the construction industry where gypsum is applied as finish for walls or as a material for interior walls in buildings, the composite described here can be applied directly, akin to general plasters, on a large variety of surfaces (plastic, aluminum, glass, and quartz). In particular, we assume that our proposed system may find use in public for self-cleaning applications in construction and building arenas.

Acknowledgements

This study was supported by the Israel Science Foundation Grant No. 12/207. We would like to acknowledge Dr Nimer Taha for his assistance with the TOC measurements.

References

1 J. Chen and C.-s. Poon, *Build. Environ.*, 2009, **44**, 1899–1906.
2 A. Fujishima, K. Hashimoto and T. Watanabe, *TiO_2 Photocatalysis: Fundamentals and Applications*, BKC, Tokyo, 1999.
3 M. R. Hoffmann, S. T. Martin, W. Choi and D. W. Bahnemann, *Chem. Rev.*, 1995, **95**, 69–96.
4 M. Janus, J. Zatorska, A. Czyżewski, K. Bubacz, E. Kusiak-Nejman and A. W. Morawski, *Appl. Surf. Sci.*, 2015, **330**, 200–206.
5 P. Ragesh, V. Anand Ganesh, S. V. Nair and A. S. Nair, *J. Mater. Chem. A*, 2014, **2**, 14773–14797.
6 L. Pinho, F. Elhaddad, D. S. Facio and M. J. Mosquera, *Appl. Surf. Sci.*, 2013, **275**, 389–396.
7 N. Shandilya, O. le Bihan, C. Bressot and M. Morgeneyer, *Environ. Sci. Technol.*, 2015, **49**, 2163–2170.
8 N. Negishi, T. Iyoda, K. Hashimoto and A. Fujishima, *Chem. Lett.*, 1995, **24**, 841–842.
9 R. Wang, K. Hashimoto, A. Fujishima, M. Chikuni, E. Kojima, A. Kitamura, M. Shimohigoshi and T. Watanabe, *Nature*, 1997, **388**, 431–432.
10 J. Yu, X. Zhao and Q. Zhao, *Thin Solid Films*, 2000, **379**, 7–14.
11 S. Guo, Z. Wu and W. Zhao, *Chin. Sci. Bull.*, 2009, **54**, 1137–1142.
12 A. H. Aïssa, E. Puzenat, A. Plassais, J.-M. Herrmann, C. Haehnel and C. Guillard, *Appl. Catal., B*, 2011, **107**, 1–8.
13 A. M. Ramirez, K. Demeestere, N. de Belie, T. Mäntylä and E. Levänen, *Build. Environ.*, 2010, **45**, 832–838.
14 A. Folli, C. Pade, T. B. Hansen, T. de Marco and D. E. Macphee, *Cem. Concr. Res.*, 2012, **42**, 539–548.
15 S. Weng, Z. Fang, Z. Wang, Z. Zheng, W. Feng and P. Liu, *ACS Appl. Mater. Interfaces*, 2014, **6**, 18423–18428.
16 J. Hu, W. Fan, W. Ye, C. Huang and X. Qiu, *Appl. Catal., B*, 2014, **158–159**, 182–189.
17 J. Hu, S. Weng, Z. Zheng, Z. Pei, M. Huang and P. Liu, *J. Hazard. Mater.*, 2014, **264**, 293–302.
18 L. Ye, K. Deng, F. Xu, L. Tian, T. Peng and L. Zan, *Phys. Chem. Chem. Phys.*, 2012, **14**, 82–85.
19 H. Gnayem and Y. Sasson, *ACS Catal.*, 2013, **3**, 186–191.
20 G. G. Briand and N. Burford, *Chem. Rev.*, 1999, **99**, 2601–2658.
21 F. J. Maile, G. Pfaff and P. Reynders, *Prog. Org. Coat.*, 2005, **54**, 150–163.
22 N. Kijima, K. Matano, M. Saito, T. Oikawa, T. Konishi, H. Yasuda, T. Sato and Y. Yoshimura, *Appl. Catal., A*, 2001, **206**, 237–244.
23 C. R. Michel, N. L. López Contreras and A. H. Martínez-Preciado, *Sens. Actuators, B*, 2012, **173**, 100–105.
24 S. Shenawi-Khalil, V. Uvarov, Y. Kritsman, E. Menes, I. Popov and Y. Sasson, *Catal. Commun.*, 2011, **12**, 1136–1141.
25 C. Karunakaran and P. Anilkumar, *J. Mol. Catal. A: Chem.*, 2007, **265**, 153–158.
26 J. Li, W. Ma, Y. Huang, X. Tao, J. Zhao and Y. Xu, *Appl. Catal., B*, 2004, **48**, 17–24.
27 H. Fu, C. Pan, W. Yao and Y. Zhu, *J. Phys. Chem. B*, 2005, **109**, 22432–22439.
28 S. Kim and W. Choi, *Environ. Sci. Technol.*, 2002, **36**, 2019–2025.
29 K.-i. Ishibashi, A. Fujishima, T. Watanabe and K. Hashimoto, *J. Photochem. Photobiol., A*, 2000, **134**, 139–142.

